

MODELING A FUEL CELL SYSTEM FOR RESIDENTIAL DWELLINGS

Except where reference is made to the work of others, the work described in this thesis is my own or was done in collaboration with my advisory committee. This thesis does not include proprietary or classified information.

Christopher P. Trueblood

Certificate of Approval:

Charles A. Gross
Professor
Electrical and Computer Engineering

S. Mark Halpin, Chair
Alabama Power Company Distinguished
Professor
Electrical and Computer Engineering

R. Mark Nelms
Professor
Electrical and Computer Engineering

Stephen L. McFarland
Acting Dean
Graduate School

MODELING A FUEL CELL SYSTEM FOR RESIDENTIAL DWELLINGS

Christopher P. Trueblood

A Thesis

Submitted to

the Graduate Faculty of

Auburn University

in Partial Fulfillment of the

Degree of

Master of Science

Auburn, Alabama

11 May 2006

MODELING A FUEL CELL SYSTEM FOR RESIDENTIAL DWELLINGS

Christopher P. Trueblood

Permission is granted to Auburn University to make copies of this thesis at its discretion, upon request of individuals or institutions and at their expense. The author reserves all publication rights.

Signature of Author

Date of Graduation

THESIS ABSTRACT

MODELING A FUEL CELL SYSTEM FOR RESIDENTIAL DWELLINGS

Christopher P. Trueblood

Master of Science, May 11, 2006
(B.E.E., Auburn University, 2004)

56 Typed Pages

Directed by S. Mark Halpin

Fuel cells produce electricity by combining hydrogen and oxygen to form water. Fuel cells have unique electrical characteristics and performances that warrant examination and discussion. From the hydrogen source to the electrical load, a polymer electrolyte membrane fuel cell system is explained and modeled with empirical equations. An ensuing simulation in Simulink exposes a fuel cell's limitations and provides avenues for successful integration into residential applications.

ACKNOWLEDGEMENTS

The author would like to thank Dr. Mark Halpin, the advisory committee, and the entire Department of Electrical Engineering for their friendliness and support of a humble graduate student. The author would also like to thank his parents, Robert and Sue Trueblood, for their admireability and unending encouragement. Lastly, the author would like to thank his best friend, Katie McCullough, for her caring and understanding.

Style manual used: Graduate School Guide to Preparation and Submission of Theses and
IEEE Power Engineering Society Format for Technical Works

Computer software used: Microsoft Word, Matlab 6.5, and Simulink

TABLE OF CONTENTS

LIST OF FIGURES	viii
I. Introduction	1
II. Motive	3
III. An Electrical Engineering Approach to Fuel Cells.....	6
IV. Fuel Cell Static Characteristics.....	9
V. Fuel Cell Dynamic Characteristics	14
VI. Power Converter	18
VII. Power Supplementation.....	21
VIII. Residential Load Conditions.....	24
IX. Incorporating the Fuel Cell System in Simulink	26
X. Fuel Cell Simulation Case Studies.....	32
XI. Conclusion	43
XII. References	44
XIII. Appendix.....	46

LIST OF FIGURES

Fig. 1. Rudimentary schematic of an individual fuel cell	2
Fig. 2. Efficiency of fuel cells and comparable power generation systems.....	4
Fig. 3. Basic Fuel Cell System Block Diagram	6
Fig. 4. Fuel cell polarization curve showing voltage/current characteristics.....	9
Fig. 5. Efficiency and cell voltage verses current density	13
Fig. 6. Power verses current density	13
Fig. 7. Electric circuit model of a fuel cell	16
Fig. 8. Power conversion block diagram	19
Fig. 9. Supplemental power source connections.....	21
Fig. 10. Simple circuit (a) and equivalent representation in Simulink (b).....	27
Fig. 11. Overall fuel cell model in Simulink	27
Fig. 12. Fuel cell subsystem.....	29
Fig. 13. Reactant flow subsystem	30
Fig. 14. Power converter subsystem	31
Fig. 15. Fuel cell stack I-V curve from simulation	33
Fig. 16. Fuel cell stack I-P curve from simulation.....	34
Table 1. Time varying load profile for first case study.....	34
Fig. 17. Power demanded from fuel cell stack for 500, 2000, and 1000 W load steps ...	35

Fig. 18. Fuel cell voltage/current response to 500, 2000, and 1000 W load steps.....	36
Fig. 19. Supplemental capacitance subsystem.....	38
Table 2. Heat pump specifications.....	39
Fig. 20. Load power profile for heat pump simulation	40
Fig. 21. Fuel cell response to heat pump simulation.....	41

I. INTRODUCTION

Fuel cell power systems have potential to meet modern society's growing energy needs. Residential dwellings, in particular, can benefit from fuel cells as a remote power source and as a backup power supply. A fuel cell system model may be examined and applied to residential applications where varying loads are prevalent.

By making water from hydrogen and oxygen, fuel cells are able to produce electrical power efficiently. The fundamentals of a typical fuel cell are illustrated in Fig. 1 [1]. Hydrogen, acting as the chemical energy source, is fed into the fuel cell to the anode and exposed to the electrolyte. A hydrogen molecule contains two electrons and two protons. Due to the unique nature of the electrolyte, only protons pass through to the cathode. Electrons remain on the anode and create an electric potential between the anode and cathode. When a load is connected as shown in Fig. 1, electrons flow from the higher potential anode to the lower potential cathode through the load and complete the circuit. Several fuel cell types have been developed by varying the electrolyte and modifying the chemical half-reactions. More detail on fuel cell types and characteristics may be found in Sections III, IV, and V.

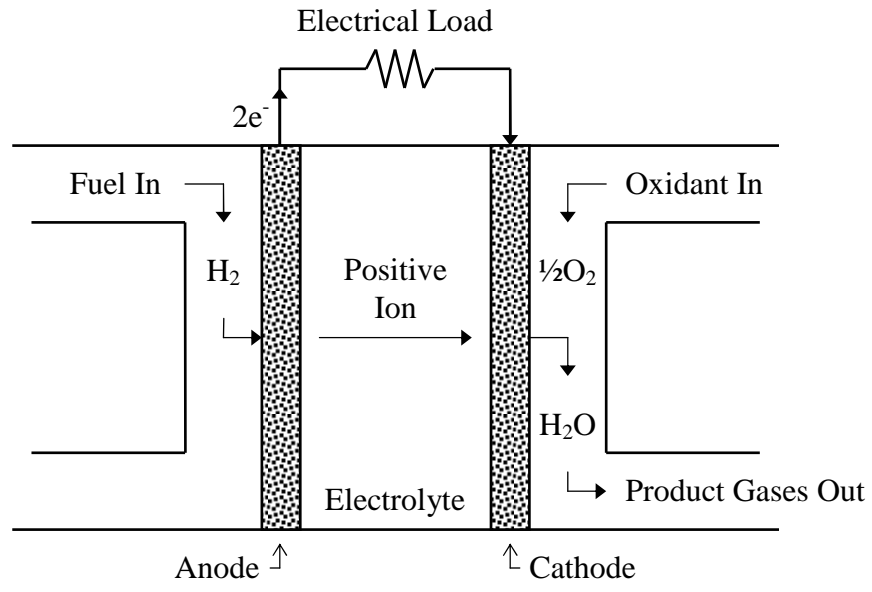


Fig. 1. Rudimentary schematic of an individual fuel cell

II. MOTIVE

A fuel cell phenomenon has captured interest from scholars since William Grove's discovery in 1839 [2]. Recently, modern fuel cell developments have emerged as a promising technology with many desirable benefits. Environmental enthusiasts look to fuel cells for their cleanliness and theoretical potential for zero emissions. As water, heat, and electricity are the only products of an ideal fuel cell system, integrating fuel cells into industrial, commercial, and residential markets nationwide gives hope to environmentalists who seek to reduce pollution and waste. Researchers and engineers look to fuel cells for their unique characteristics. Fuel cells can be scaled down to fit inside a mobile phone and scaled up to sit on a city block, producing megawatts [3]. The size of a fuel cell system does not directly affect its efficiency because no mechanical or thermodynamic processes occur inside a fuel cell. Only chemical reactions occur, allowing fuel cells to exceed efficiency limitations of internal combustion engines and gas turbines, as these heat engines are limited by the Carnot cycle. Fuel cell and heat engine efficiencies over a range of power generation levels are compared in Fig. 2. Note that Fig. 2 represents technologies as of November 2004, and the given efficiencies are based on the lower heating value (LHV) of the fuel [1].

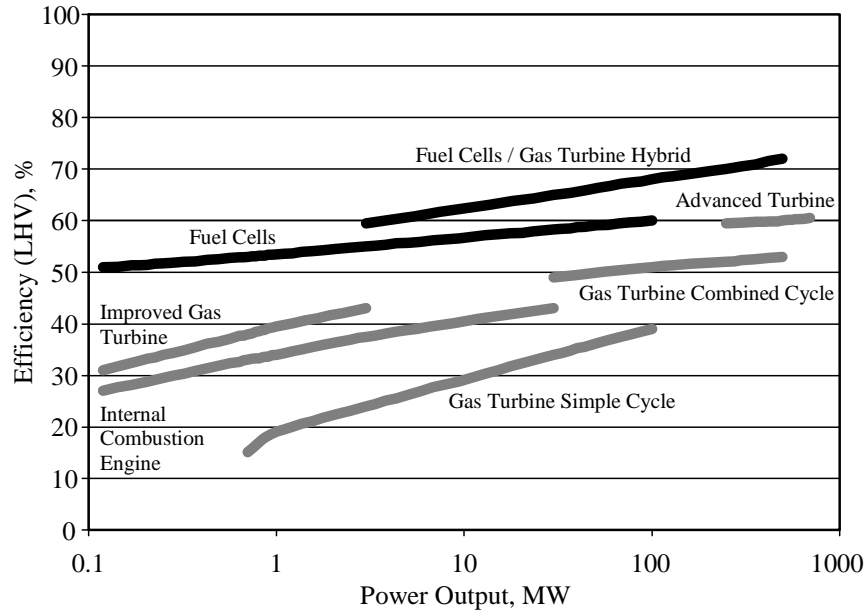


Fig. 2. Efficiency of fuel cells and comparable power generation systems

Not only do fuel cells surpass heat engines in efficiency, they also surpass batteries in energy density. A typical fuel cell system may be more than ten times as energy dense than a comparable lithium battery system [4], challenging researchers and engineers to develop smaller and lighter power sources for handheld electronics and transportation. Additionally, fuel cells have no moving parts, allowing them to operate quietly and more reliably than conventional generators [3]. When integrated into stationary applications, quality heat produced from a fuel cell can be used to heat water and warm a building.

Those who view fuel cells as an efficient, environmentally friendly power source of the future cannot overlook the most challenging shortcoming of fuel cell systems. Hydrogen production and storage currently restricts fuel cell markets by its high cost and undeveloped infrastructure. Hydrogen may be reformed from hydrocarbon fuels, such as natural gas, methane, and gasoline, resulting in a costly and pollutive energy source [3]. For comparison, a fuel cell system powered by reformed natural gas releases about one-

third less carbon dioxide than an internal combustion engine generating equivalent power. Alternatively, extracting hydrogen from water through electrolysis requires an electrical source and is generally about 65 to 75 percent efficient. Solar or wind power may be used to perform environmentally friendly electrolysis but is cost prohibitive. Several fuel cell systems take advantage of the fossil fuel infrastructure by including onboard reformers so that natural gas or other hydrocarbon fuel may be supplied at the point of use. However, until an infrastructure for hydrogen production and storage develops, fuel cell systems will remain aloof.

Besides lacking a hydrogen infrastructure, fuel cells present many engineering challenges. A fuel cell or stack of fuel cells cannot be instantaneously turned on. Some types, such as the solid oxide fuel cell, operate at temperatures exceeding 600° C. These high temperature fuel cells take at least several hours to turn on. Low temperature fuel cells, such as the polymer electrolyte membrane fuel cell, operate below the boiling point of water and take only a few minutes to turn on. Regardless of the fuel cell type, fuel cells do not respond well to power transients that occur in supplying a dynamic load. Under rapid load changes, such as starting a heat pump or accelerating quickly in an automobile, the fuel cell alone may not be able to provide adequate power. Fuel cell systems must be engineered so that they can be used both as stationary and mobile power sources to meet society's dynamic electric loads. The fuel cell system model examined in this thesis centers around residential end-use.

III. AN ELECTRICAL ENGINEERING APPROACH TO FUEL CELLS

Engineering a fuel cell system in its entirety requires extensive knowledge of all components that link a fuel source to an electrical load. The elementary system shown in Fig. 3 depicts a typical fuel cell system that can be divided into chemical, mechanical, and electrical components.

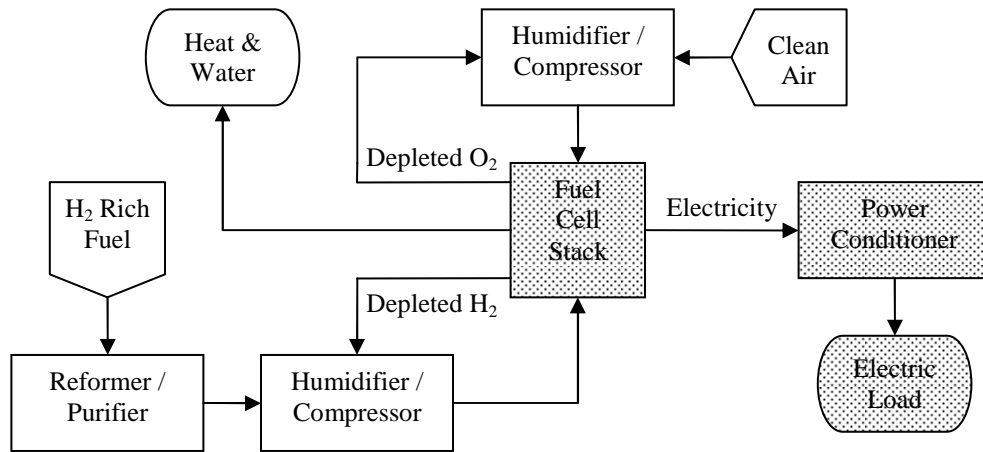


Fig. 3. Basic Fuel Cell System Block Diagram

In most fuel cell systems, hydrogen must be reformed from the source fuel, purified, humidified, and compressed before it can enter the fuel cell stack. Humidified and compressed oxygen or air is also needed to enter the fuel cell stack. As the electrical engineering associated with these chemical and mechanical processes is minimal, a basic understanding is necessary only for completeness. To electrically engineer the system, an engineer must have appreciable knowledge of the fuel cell stack performance, power conditioning electronics, and load characteristics. These three sections, shown as shaded blocks in Fig. 3, are detailed in Sections IV, V, VI, VII, and VIII.

A fuel cell stack's details, characteristics, and performances vary among different types of fuel cells. Fuel cells are generally classified by the type of electrolyte used, primarily because the electrolyte dictates the fuel cell's operating temperature range [1]. The operating temperature, in turn, dictates the amount of fuel processing required (reforming and purifying) and the startup time of the system [1]. The electrolyte also affects the half-reactions taking place within the fuel cell. In some fuel cells, water is produced on the anode side of the cell rather than the cathode side. Nevertheless, the overall chemical reaction remains the same:



The most popular and widely available fuel cell is the polymer electrolyte membrane fuel cell (PEMFC). Using a solid polymer ion exchange membrane, the electrolyte is an excellent proton conductor [1]. The polymer must be kept at temperatures below 100° C, making thermal management important, and requires at least 99.99% pure hydrogen to reduce the potential for contaminating the membrane. Because a PEMFC operates between 0° C and 100° C, it has the most rapid startup time (about a minute or two) of all fuel cells. PEM fuel cells are able to respond quicker to dynamic loads than other fuel cell types and operate with an electrical efficiency ranging from 40 to 60 percent [1].

The second most popular fuel cell is the solid oxide fuel cell (SOFC). The electrolyte consists of a solid ceramic, nonporous metal oxide and operates between 500° C and 1000° C. Because SOFCs operate at high temperatures, they assist with internal fuel reformation, allowing non-pure hydrogen rich fuels. However, thermal expansion and sealing mismatches make fabricating the cell difficult. Solid oxide fuel cells have such a long startup time (several hours or more) making them only practical

for powering loads that are always on. Solid oxide fuel cells operate with electrical efficiencies ranging from 40 to 60 percent.

The remaining three major types of fuel cells are molten carbonate fuel cells, alkaline fuel cells, and phosphoric acid fuel cells. None of these three types are as popular as the PEM fuel cell, but their characteristics are worth noting for completeness. Molten carbonate fuel cells (MCFC) have an alkali carbonate electrolyte that forms a highly conductive molten salt but only at about 650° C. A carbon dioxide source is required for this fuel cell, and CO_3^{2-} plays a key role in the fuel cell's half reactions. Aside from the internal chemical reactions, a MCFC portrays similar characteristics to a SOFC [1]. Alkaline fuel cells (AFC) use concentrated potassium hydroxide as the liquid electrolyte and operate between 50° C and 200° C. Carbon dioxide poisons the sensitive electrolyte, so alkaline fuel cells are mostly successful in space applications [1]. Lastly, as the name suggests, phosphoric acid fuel cells (PAFC) use liquid phosphoric acid as the electrolyte. These fuel cells operate at about 200° C, produce electricity about 40 percent efficiently, and were “the first fuel cells to cross the commercial threshold in the electric power industry” [3].

IV. FUEL CELL STATIC CHARACTERISTICS

Because the PEMFC is the most popular and has the highest technology-readiness level [5], it will be used as the example fuel cell for the remainder of this thesis.

Regardless of the type of fuel cell used in a system, fuel cells loosely exhibit similar electric performance. The electric potential realized between the anode and cathode varies primarily with the amount of current drawn from the fuel cell stack (temperature and pressure also affect the fuel cell's performance). The voltage/current relationship (polarization curve) for a single fuel cell, adapted from [1], is shown in Fig. 4.

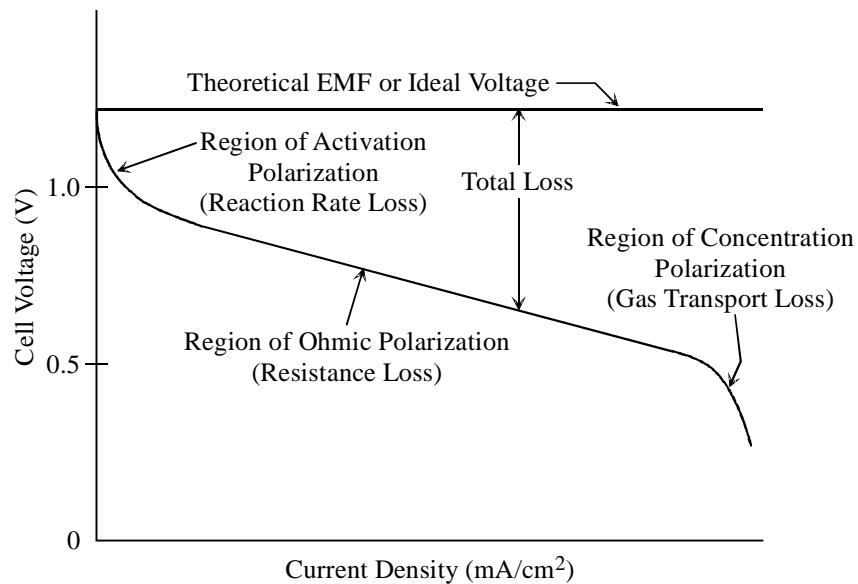


Fig. 4. Fuel cell polarization curve showing voltage/current characteristics

If the fuel cell performed as an ideal voltage source, then the polarization curve would match the horizontal theoretical EMF line for all current densities. The ideal or

equilibrium voltage (E_{eq}) varies with temperature and pressure, defined by the following modified Nernst equation [6]:

$$E_{eq} = -\frac{\Delta G}{2 \cdot F} + \frac{\Delta S}{2 \cdot F} \cdot (T - T_{ref}) + \frac{R \cdot T}{2 \cdot F} \cdot \ln\left(\frac{P_{H_2} \cdot P_{O_2}^{1/2}}{P_{H_2O}}\right) \quad (2)$$

In the above equation, ΔG is the change in Gibbs free energy or usable energy associated with the reaction, F is Faraday's number (96,485 C/mol), ΔS is the change in entropy, T is the fuel cell temperature on the Kelvin scale, T_{ref} is the reference temperature or room temperature (298.15 K), and R is the molar gas constant (8.3145 J/K·mol). The first term (containing ΔG) represents the theoretical voltage at room temperature determined from Faraday's Law. This value is a constant 1.229 V when hydrogen and oxygen react to form water. The second term of the equation (containing ΔS) accounts for changes in absolute temperature with respect to standard conditions [7]. The last term accounts for product and reactant activities, as defined by Nernst. The variables P_{H_2} , P_{O_2} , and P_{H_2O} represent the partial pressures of hydrogen, oxygen, and water vapor, respectively, usually measured as a fraction of standard pressure. These pressures can affect the dynamic response of the fuel cell and are detailed in Section V. The resulting equation for E_{eq} with only temperature and pressure variables is:

$$E_{eq} = 1.229 - (8.5 \times 10^{-4}) \cdot (T - 298.15) + (4.308 \times 10^{-5}) \cdot T \cdot \ln\left(\frac{P_{H_2} \cdot P_{O_2}^{1/2}}{P_{H_2O}}\right) \quad (3)$$

The equilibrium voltage can occur only when no current flows from the fuel cell. A typical fuel cell stack may contain many individual cells connected in series, resulting in an ideal stack voltage that is a multiple of E_{eq} . The direct current flowing out of a fuel cell varies directly with the electrodes' areas. For evaluating a fuel cell's characteristics,

the current is normalized to a current density as shown on the abscissa axis of Fig. 4. The curve in Fig. 4 can be divided into three polarization regions: activation, ohmic, and concentration [1]. These operating regions affect the fuel cell's voltage and consequently, its efficiency. The specific polarization factors are considered overpotentials (V_{act} , V_{ohmic} , and V_{conc}) and negatively contribute to the fuel cell's voltage. The resulting voltage between the anode and cathode is:

$$V_{cell} = E_{eq} - V_{act} - V_{ohmic} - V_{conc} \quad (4)$$

Each overpotential term varies with current, temperature, and pressure. The concentration overpotential (V_{conc}) is pronounced at high currents yet is negligible in the activation and ohmic regions. Furthermore, operating a fuel cell in the concentration region results in a rapid decrease in power output and efficiency, and it increases the risk of damaging the cell [1]. Fuel cells are not operated in this region, allowing the concentration overpotential term to be ignored completely [5]. The activation overpotential (V_{act}) occurs because the reaction kinetics are sluggish, as a certain activation energy must be overcome for the reaction to occur. The activation overpotential is represented as a function of time as an empirical equation [6]:

$$v_{act} = \xi_1 + \xi_2 \cdot T + \xi_3 \cdot T \cdot \ln C_{O_2} + \xi_4 \cdot T \cdot \ln i \quad (5)$$

The coefficients (ξ_i) are parameters unique to an individual fuel cell. The variable i represents the fuel cell operating current, and C_{O_2} is the concentration of oxygen, defined as [6]:

$$C_{O_2} = P_{O_2} \cdot 1.97 \times 10^{-7} \cdot e^{498/T} \quad (6)$$

The remaining overpotential, V_{ohmic} , accounts for the fuel cell's resistance to electrons flowing through the electrodes, resistance to ions flowing through the electrolyte, and contact resistance. Using Ohm's Law, this overpotential is directly proportional to the product of the fuel cell's internal resistance and current, and may be expressed as [6]:

$$V_{ohmic} = R_{ohmic} \cdot i = (\xi_5 + \xi_6 \cdot T + \xi_7 \cdot i) \cdot i \quad (7)$$

The parameters ξ_6 and ξ_7 are two or three orders of magnitude smaller than ξ_5 , resulting in a nearly linear ohmic polarization region.

By knowing the voltage/current relationships, a fuel cell's efficiency and power characteristics can be determined. The efficiency of a fuel cell can be calculated from the following equation from [1] and [7]:

$$\eta = \frac{\Delta G}{\Delta H} \cdot \mu_f \cdot \frac{V_{cell}}{E_{eq}} \quad (8)$$

The variable ΔH is the change in enthalpy of the reaction, and the variable μ_f represents the fuel utilization percentage to account for the amount of fuel that is actually converted in the fuel cell [1]. The quotient of ΔG and ΔH under standard conditions is 0.830, indicating that an ideal fuel cell can be at most 83% efficient [1]. For illustrative purposes, the Ballard Mark V fuel cell, operated under standard conditions with 95% fuel utilization, has the following efficiency/voltage relationship [7]:

$$\eta = 0.641 \cdot V_{cell} \quad (9)$$

The resulting efficiency curve overlays the polarization curve when scaled appropriately as shown in Fig. 5, adapted from [7]:

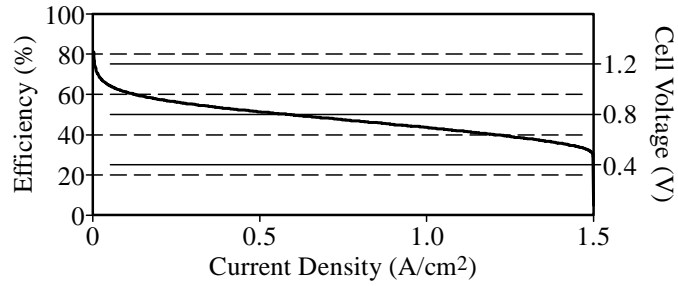


Fig. 5. Efficiency and cell voltage verses current density

A fuel cell's electrical power output is the product of the cell voltage and current. The power characteristics over the fuel cell's operating range may be expressed in terms of power density, as shown in Fig. 6 for the Ballard Mark V fuel cell [7].

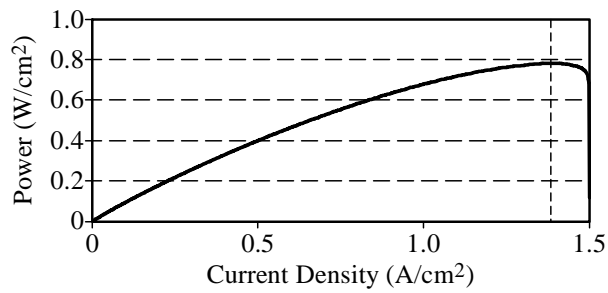


Fig. 6. Power verses current density

The dashed vertical line crosses the fuel cell's maximum power point and thus sets the practical operating limit for the fuel cell.

V. FUEL CELL DYNAMIC CHARACTERISTICS

Knowing the fuel cell's voltage, current, efficiency, and power relationships are necessary for electrically engineering a fuel cell system. However, the above description did not account for the fuel cell's dynamic response. Fuel cells exhibit a characteristic called charge double layer capacitance [7]. When hydrogen is split apart in the electrode/electrolyte interface (part of the membrane electrolyte assembly), hydrogen's electrons collect on the electrode's surface and its protons are drawn to the electrolyte. An electric charge accumulates on or near the electrode/electrolyte interface and acts as an electrical capacitor. The effect of this charge double layer capacitance is significant when the fuel cell's current changes due to a dynamic load [6]. As the voltage across a capacitor cannot change instantaneously, a fuel cell's voltage will not immediately follow its current. The delayed voltage change affects the activation overpotential but not the ohmic overpotential. This delay may be represented as a capacitor paralleled with a resistor, yielding a time constant (τ) of [7]:

$$\tau = C \cdot R_{act} \quad (10)$$

The variable R_{act} represents the activation resistance, determined by dividing the steady state activation overpotential by the fuel cell current [7]:

$$R_{act} = \frac{v_{act}}{i} \quad (11)$$

The capacitance, C , is determined by the physical properties of the fuel cell and typically equals to a few farads for an entire fuel cell stack [6].

Another noteworthy characteristic of a fuel cell stack is its reactant flow dynamics. To consider these dynamics, including effects of reactant partial pressures, the following operating conditions are assumed. Hydrogen is provided to the anode inlet at a constant pressure. Excess or unused hydrogen is recirculated from the anode outlet to the anode inlet. Additionally, air is supplied at a constant pressure to the cathode. If the fuel cell current increases, the reactant consumption rate would also increase, resulting in an implied reduction in partial pressures [5]. In fact, the current drawn from a fuel cell directly determines the quantity of hydrogen and oxygen that are needed to react inside the stack and to maintain an energy balance [5]. For a fuel cell, the relationship between the rate of hydrogen consumption and the fuel cell current is [5]:

$$\dot{m}_{H_2,used} = \frac{i}{2 \cdot F} \quad (12)$$

The variable $\dot{m}_{gas,used}$ represents a gas's consumption rate in moles per second, and F is Faraday's number. Likewise, the expression for oxygen consumption is [5]:

$$\dot{m}_{O_2,used} = \frac{i}{4 \cdot F} \quad (13)$$

For dynamic analysis, the ideal gas law and mole conservation principle may be utilized. The generic equation relating reactant flow with the derivative of partial pressure is [8]:

$$\frac{d}{dt} p_{gas} = \frac{R \cdot T}{Vol} (\dot{m}_{gas,in} - \dot{m}_{gas,out} - \dot{m}_{gas,used}) \quad (14)$$

The symbol *Vol* is used to represent the anode/cathode volume instead of *V* so that it is not confused with voltage. The reactant flow rate in to the anode/cathode ($\dot{m}_{gas,in}$) is a known quantity and will be considered as a constant for dynamic analysis. The reactant flow rate out of the anode/cathode ($\dot{m}_{gas,out}$) may be obtained from a feedback loop when

the above equation is simulated as a control system. By solving the above differential equation using Laplace transformations for each gas, the partial pressures for hydrogen, oxygen, and exhaust vapor can be determined and substituted into the Nernst equation to determine E_{eq} [9].

An equivalent circuit model of a fuel cell can be assembled from knowing a fuel cell's polarization curve and dynamic response characteristics. The schematic shown in Fig. 7 presents such a model [6].

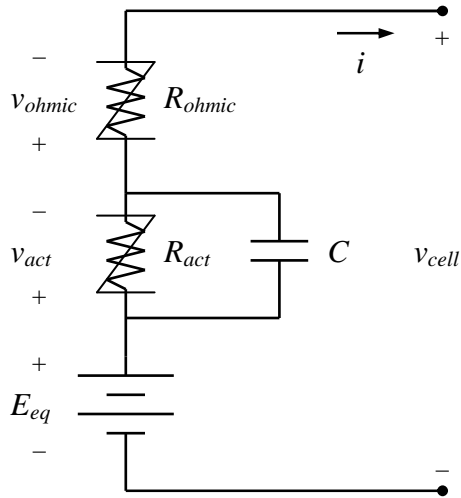


Fig. 7. Electric circuit model of a fuel cell

The activation voltage under steady state conditions may be taken directly from the equation presented for v_{act} in Section IV because the double layer capacitance resembles an open circuit in steady state. However, to represent the activation voltage dynamics, the double layer capacitance, C , must be considered in parallel with the activation resistance, R_{act} . Therefore, the true representation of the activation voltage is:

$$v_{act} = R_{act} \cdot \left(i - C \frac{dv_{act}}{dt} \right) \quad (15)$$

The complete fuel cell circuit model may now be connected to the power conditioner subsystem. Power conditioning theory for inclusion in a fuel cell system model is detailed in Sections VI and VII.

VI. POWER CONVERTER

Power conditioning electronics are necessary to connect a fuel cell source to an electric load. The low dc voltage produced by a fuel cell coupled with its limited peak power capabilities prevent fuel cells from being directly connected to many loads. For residential applications, most electric loads require a single-phase ac voltage source of either 120 V or 240 V RMS. Furthermore, loads requiring large amounts of power to start, such as motors and compressors, will consume more power on startup than properly rated fuel cells can provide. The power conditioning unit of the fuel cell system can be divided into two sections: power conversion from low voltage dc to high voltage ac and power supplementation to aid in supplying peak power to a load.

A typical fuel cell's voltage may range from about 1.2 V open circuit to 1.0 V under light loading to 0.5 V under heavy loading. This wide voltage swing is magnified when many fuel cells are stacked together and connected in series. A fuel cell stack may contain about 50 individual cells for kilowatt units or more than 100 cells for larger stacks. Fuel cell stacks may be connected in parallel for increased power output, as parallel arrangements will increase the current output of the source without increasing the stack voltage. Considering a single fuel cell stack with 50 cells, the general operating voltage may range from 25 V to 50 V – a factor-of-two voltage variation. The fuel cell stack's widely varying voltage must be converted to single phase, three-wire 240 V ac to power a residential load. Power conversion of this nature can be broken into two stages, shown in Fig. 8:

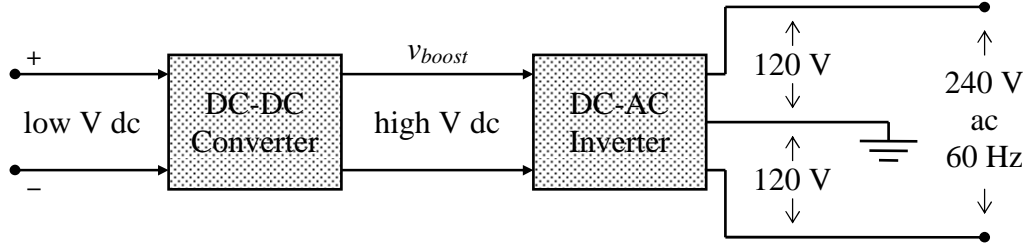


Fig. 8. Power conversion block diagram

It is possible to rearrange the converters shown in Fig. 8 so that low voltage dc is converted to low voltage ac, followed by a low voltage ac to high voltage ac conversion. However, this dc-ac-ac configuration is larger and more costly than the dc-dc-ac configuration shown in Fig. 8 [10]. Furthermore, having a high voltage dc link between the fuel cell and load allows supplemental power sources to be connected to a constant dc bus. Many types of dc-dc boost converters and dc-ac inverters exist. For the purposes of modeling a fuel cell system, both converters may be analyzed without detailing specifics of the internal MOSFETs, IGBTs, transformers, and inductors that are typically found inside such converters. Rather, both converters may be viewed as single entities where the output is a function of the input. In this case, the dc-dc boost converter may be expressed as a set of equations in the Laplace domain [11]:

$$V_{boost}(s) = \frac{V_{stack}(s)}{1 - D} \quad (16)$$

$$D = \left(k_{P,DC} + \frac{k_{I,DC}}{s} \right) \cdot (V_{boost,ref} - V_{boost}(s)) \quad (17)$$

The duty ratio, D , is regulated with a PI controller (with proportional and integral coefficients k_P and k_I , respectively) fed from the output error (voltage difference between a predefined reference/desired voltage and the actual output). If D is zero, no voltage

conversion takes place; if D is near 80%, maximum voltage boost occurs. Similarly, the dc-ac inverter may be expressed as a set of equations [11]:

$$v_{AC} = m \cdot v_{boost} \cdot \sin(2\pi \cdot 60 \cdot t) \quad (18)$$

$$m = \left(k_{P,AC} + \frac{k_{I,AC}}{s} \right) \cdot (V_{AC,ref} - V_{AC}(s)) \quad (19)$$

The output voltage, v_{AC} , relies on another PI controller to regulate the modulation index, m . Like the boost converter duty ratio, the inverter modulation index varies between zero and one. The inverter can only produce an ac voltage peak less than or equal to the input dc voltage (v_{boost}). Many inverters are designed to output the desired ac voltage at a modulation index of about 0.8 so that the output voltage can rise, if needed, in response to transients. The above equations depict a lossless boost converter and inverter. To simulate the power loss incurred by the converters, the power output may be divided by the collective efficiencies of the boost converter and inverter.

VII. POWER SUPPLEMENTATION

The second section of the fuel cell system's power conditioning unit consists of power supplementation to aid in supplying peak power to a load. To accomplish this goal, one or more temporary energy storage mediums must be employed. The three most common and practical sources for supplemental power are ultracapacitors, batteries, and the power grid. Preferred connections for each supplemental power source are illustrated in Fig. 9.

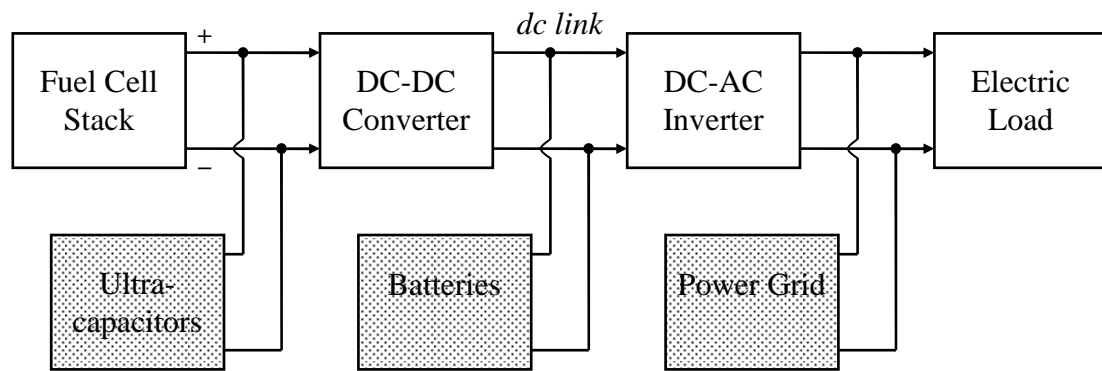


Fig. 9. Supplemental power source connections.

An ordinary capacitor may not be powerful enough to supply adequate supplementary power for a residential fuel cell system. Many technological advances in electrochemistry have given rise to ultracapacitors. These devices are constructed similar to batteries in that the terminals are two electrodes immersed in a separated electrolyte. Unlike battery electrodes, ultracapacitor electrodes have an extremely high surface area, often 500 to 2,000 m²/g, allowing them to discharge high power levels [11]. Such ultracapacitors range in capacitance from 10 F to 2,700 F but operate at very low voltage

(around 2.5 V) [11]. Ultracapacitors are best suited for parallel connection at the lowest system voltage level, namely, the fuel cell terminals as shown in Fig. 9. For connection in parallel with a fuel cell, many ultracapacitors need to be connected in series simply to adhere to the voltage rating of individual capacitors. These capacitor banks must be individually balanced, either actively or passively, so that the capacitors do not exceed their voltage ratings [11].

Ultracapacitors have higher power densities than batteries, yet batteries have higher energy densities than ultracapacitors. Therefore, a battery pack is well suited to aid a fuel cell in moderate and elongated power supplementation. Many battery types are well developed, such as lead-acid, nickel metal hydride, and lithium ion. For stationary applications where mass and volume are not critical factors, lead-acid batteries may be the preferred type due to their low cost. Regardless of the type of battery used, no battery pack can be directly connected in parallel with a fuel cell. Voltage mismatches due to the fuel cell stack's and battery pack's independent voltage fluctuations indicate that a practical battery pack must be connected to the high voltage dc link between the boost converter and inverter, as shown in Fig. 9. Battery packs often exceed 200 V and may maintain voltages high enough so that the battery pack itself can serve as the boost converter's reference voltage. For example, a single 12 V lead-acid battery may operate at 10.5 V when nearly discharged. A pack of twenty nearly-discharged batteries will result in a 210 V pack. If the pack voltage serves as the dc link voltage, then the inverter will be able to supply 120 V ac RMS at 81% modulation, indicating that the power conditioner subsystem can adequately supply a typical household electric load when the supplemental battery pack is nearly empty. Additionally, a battery pack must be

connected to the dc link via a charge controller so that the batteries will be charged and discharged according to their ratings.

The third common supplemental power source is the power grid. If the power conditioner subsystem is synchronized with the power grid, then it can operate in parallel with a local distribution line, as shown in Fig. 9. Any supplemental power needed will flow seamlessly to the load, eliminating the need for ultracapacitors and batteries.

However, stationary fuel cell systems are mostly considered for remote, off-grid locations or for backup power when the grid is down. In these cases, the supplemental power grid connection is no longer an option. The analysis in this thesis assumes that a power grid connection is not available.

VIII. RESIDENTIAL LOAD CONDITIONS

Because a fuel cell's purpose is to power an electric load, having an understanding of the load characteristics is critical to a fuel cell system's success. The electrical load in residential dwellings varies widely throughout a typical day. Over fifty percent of residential energy is used for heating, ventilation, and air conditioning (HVAC), hot water, and refrigeration [12]. The remaining energy used in a household may come from cooking appliances, lighting, convenience appliances, such as washing machines and dishwashers, and personal electronics, such as computers and televisions. A mid-sized house (about 2,500 ft²) typically draws 1.9 kW average power daily, with peaks varying from 9 kW to 15 kW [12]. Daily residential power consumption may be classified into three categories based on loading conditions: startup transients, short-term loads, and long-term loads.

Startup transients occur when large motors start. HVAC units and vacuum cleaners, among other motor-driven appliances, create brief power surges when turned on. These motor-starting transients generally last less than five seconds, but cause residential power consumption to reach a maximum. The most severe startup transients originate from HVAC systems. A mid-sized house may have a 3-ton (10.6 kW) heat pump that pulls over 15 kW the instant the unit's compressor turns on. Although this particular startup transient is large, the peak power surge lasts only fractions of seconds and decays rapidly as the motor begins to turn. A fuel cell's supplemental ultracapacitors

could aid in supplying peak power during startup transients as demonstrated in the second case study of Section X.

The second power demand category is short-term loading. Many power hungry appliances operate only for fractions of hours, leading to the consideration of short-term loading characteristics for a residence. A heat pump normally does not run continuously for more than several minutes, nor do hair dryers or refrigerators. However, when devices such as these operate, they draw noticeably large amounts of power. For example, a 0.7 kW washing machine, a 1.4 kW vacuum cleaner, a 1.8 kW hair dryer, a 4.5 kW hot water heater, and a 4.5 kW air conditioning unit may run simultaneously on a given day. These devices consume 12.9 kW collectively, but each one operates continuously for only fractions of an hour, fitting the necessary characteristic for short-term loading. Fuel cell systems must be able to supply short-term power requirements when scenarios like the one mentioned occur. A fuel cell's supplemental batteries could contribute most of the supplemental power during short-term loading intervals.

The third power demand category is long-term loading. Ovens, lights, televisions, and computers are examples of loads that may operate for an hour or more in residential dwellings. The power demanded during long-term loading is less than the power demanded during transient and short-term conditions. Therefore, a properly rated fuel cell could charge the supplemental battery pack during long-term loading. A fuel cell system, at minimum, must be able to supply long-term loads without any supplemental power sources.

IX. INCORPORATING THE FUEL CELL SYSTEM IN SIMULINK

The mathematical equations for a fuel cell and power conditioner presented in the previous sections may be modeled and simulated using a computer. The fuel cell model alone can be examined for its response characteristics due to various dynamic loads. More importantly, the fuel cell system model may be used to evaluate necessary supplemental power requirements for residential loading, leading to optimal selection of ultracapacitors and batteries. The MathWorks' simulation and modeling package, Matlab and Simulink, provides an appropriate software tool for simulating the complexities of a fuel cell system. Simulink models consist of blocks connected by signal lines. A block's output signal is a function of its input signal and may be a simple math operation, a user-defined expression, a transfer function in another domain, or many others. Simulink treats all inter-block signals in the time domain and seamlessly converts signals to and from other domains, such as the Laplace and Z domains, when controllers, integrals, or transfer functions are used. Creating electrical circuits in Simulink poses several challenges. The signal lines connecting blocks are simply numbers or arrays of numbers. Therefore, a single signal line can either represent a voltage or a current, but not both. Electric circuit analysis in Simulink must be modeled as a system of equations. A demonstration of Ohm's Law can be modeled as shown in Fig. 10:

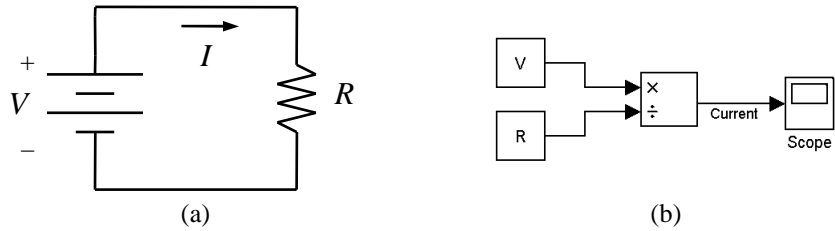


Fig. 10. Simple circuit (a) and equivalent representation in Simulink (b)

Simulink does include a power system blockset, *SimPowerSystems*, where actual circuit elements like the one in Fig. 10a may be drawn and analyzed. However, the *SimPowerSystems* blocks are extremely processor intensive and result in undesirably long simulation run times. The fuel cell system presented in this text is modeled using standard blocks.

The fuel cell system model consists of two major subsystems, the fuel cell stack and the power converter. A time dependent load, realized as a varying resistance, serves as the model's input. The outputs, shown in the overall system model in Fig. 11, include the power demanded by the load and power delivered by the fuel cell.

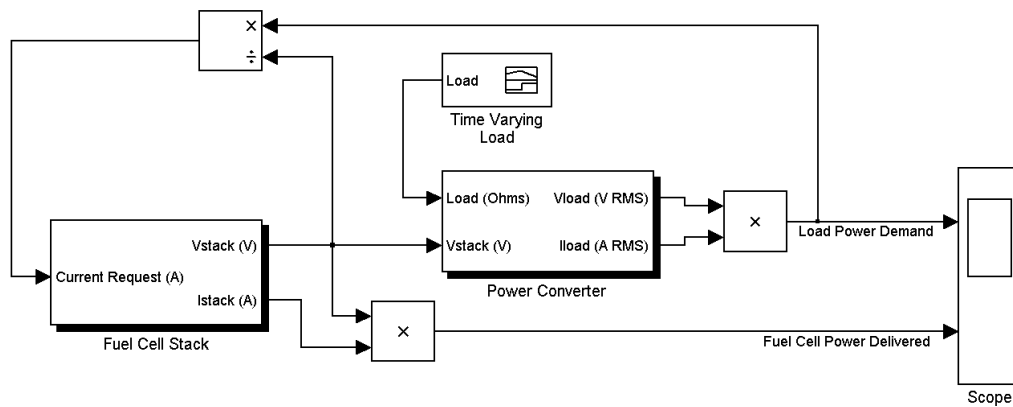


Fig. 11. Overall fuel cell model in Simulink

When the simulation begins, the time varying load resistance is fed into the power converter, along with the initial fuel cell stack voltage. The power converter outputs an ac voltage and current required to supply the load. Additionally, the power converter implements appropriate power conversion and scaling based on the fuel cell stack voltage. The output load voltage and current signals are used to calculate the load power needed to be drawn from the fuel cell stack. When divided by the stack voltage, the load power demand translates into a dc current request and feeds back into the fuel cell stack. The fuel cell stack subsystem models the circuit from Fig. 7 by evaluating all underlying equations that govern the stack voltage output. The dynamically changing stack voltage is sent back to the power converter to close the loop. The difference between the load power demanded and the fuel cell's power delivered results in the amount of supplemental power needed to satisfy the load completely.

The fuel cell stack subsystem consists of blocks and signals that implement the fuel cell equations discussed in Sections IV and V, accounting for steady state and dynamic conditions. The fuel cell subsystem is shown in Fig. 12.

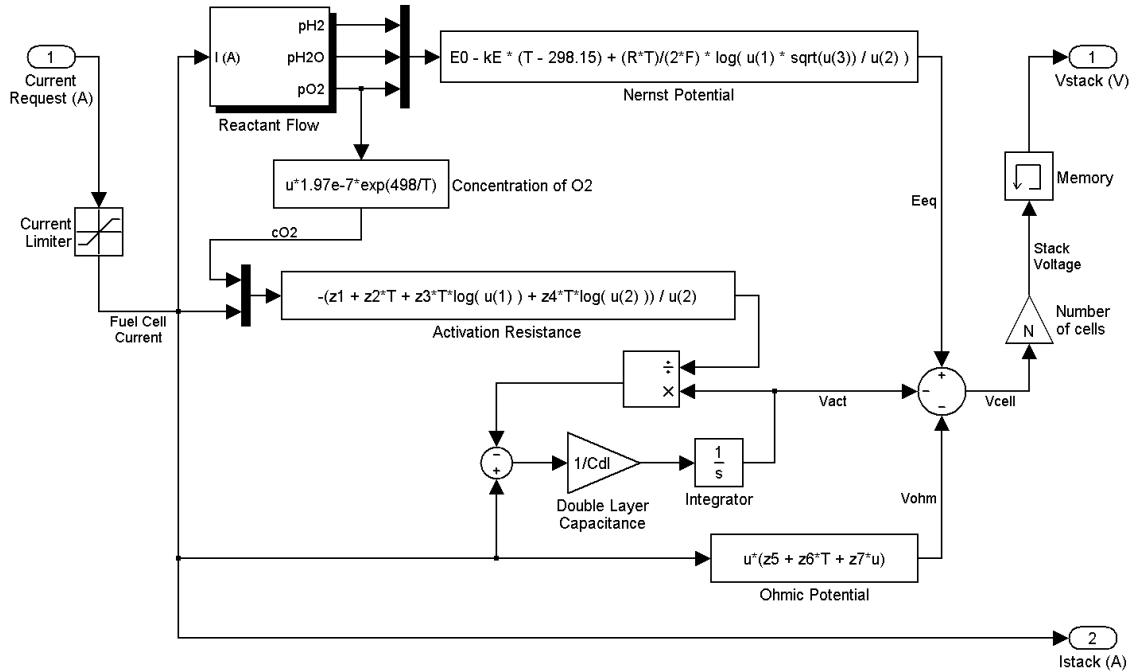


Fig. 12. Fuel cell subsystem

Several blocks in the fuel cell subsystem warrant discussion. The input current request must pass through a limiter, as the fuel cell's maximum current draw cannot be exceeded. Additionally, the current request must be positive because the fuel cell is designed to operate only as a power source. The modeled fuel cell current cannot equal zero because it is used in a natural log function to calculate activation resistance. The blocks containing user-defined expression utilize the variable u or $u(i)$ to represent the input signal. The Nernst potential and activation resistance blocks take multiple inputs and require the incoming signals to be multiplexed, illustrated by the thick vertical bar. As the fuel cell equations are for a single fuel cell, the output voltage must be scaled by the number of cells, N , to represent the entire stack voltage. The memory block is present at the output only to provide an initial condition for stack voltage. The reactant flow

subsystem, shown in Fig. 13, models the hydrogen activity in the anode and the oxygen and water vapor activities in the cathode.

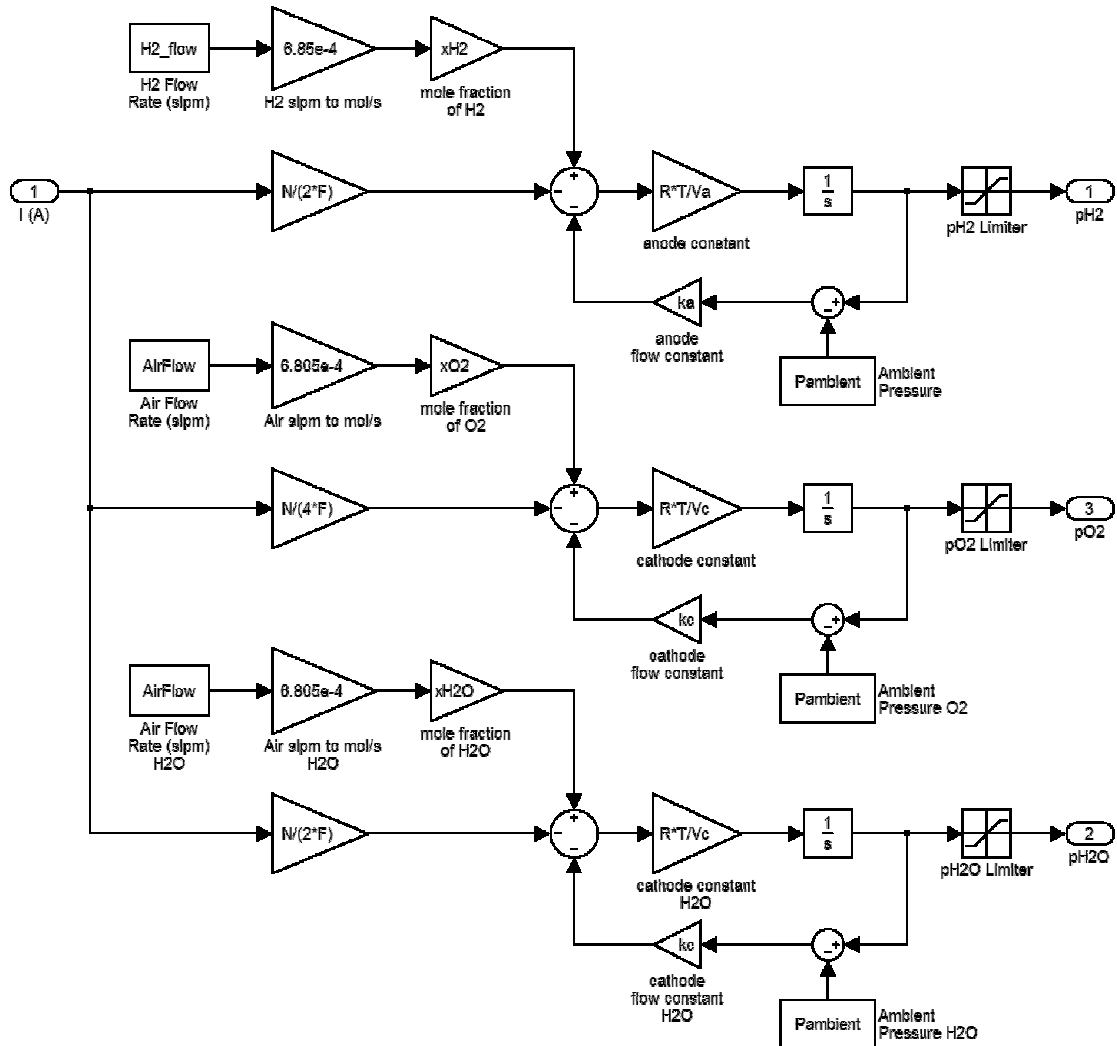


Fig. 13. Reactant flow subsystem

As described in Section V, the hydrogen and airflow rates are held constant, and the input current request dictates the amount of reactant needed, thus affecting its partial pressure.

The blocks in the reactant flow subsystem implement the partial pressure differential equations for hydrogen, oxygen, and water vapor. Limiters are placed on the output partial pressures to simulate practical pressure limitations inside the fuel cell stack.

The power converter subsystem, shown in Fig. 14, models the dc-dc boost converter and the dc-ac inverter described in Section VI.

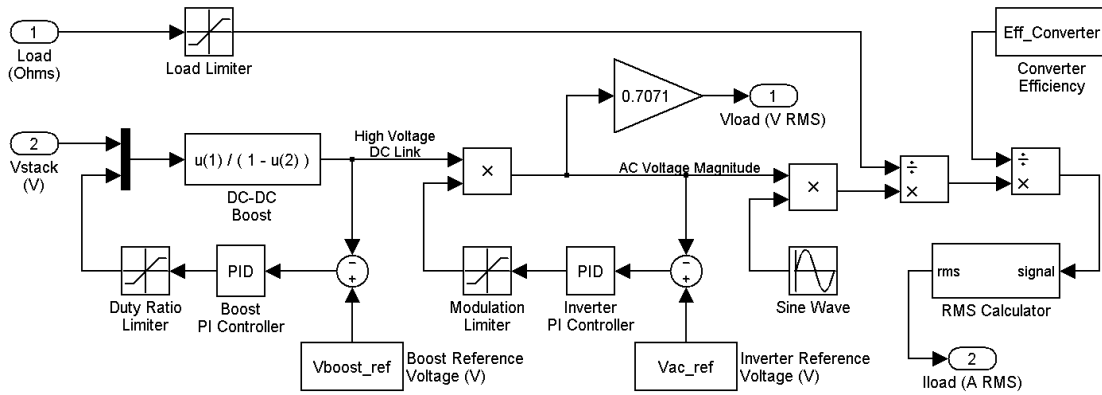


Fig. 14. Power converter subsystem

The load resistance, serving as the system input, is divided into the inverter ac voltage to generate a load current. Furthermore, the boost converter and inverter efficiencies are factored into the model by scaling the load current appropriately. The corresponding load power profile (or power demanded by the load) may be determined by multiplying the ac output voltages and currents over the duration of the simulation.

X. FUEL CELL SIMULATION CASE STUDIES

To demonstrate the fuel cell system model simulation, two case studies are presented. The first simulation case study examines the fuel cell's current-voltage (I-V) polarization curve, current-power (I-P) curve, and dynamic response to a variable step load. The general fuel cell parameters match those from other sources, [5], [7], [9], and [13], whose authors have parameterized the Ballard Mark V fuel cell stack. Reactant flow parameters were adopted from [5] and [9], and power conditioner parameters were adopted from [11] and [14]. These parameters are listed in the Appendix using Matlab syntax. To simulate the fuel cell stack's I-V curve, the overall system shown in Fig. 11 was modified by breaking the fuel cell stack's current request feedback signal. The current request can now be fed directly by a source block so that currents, ranging from zero to 300 A, could be explicitly applied to the fuel cell stack. The fuel cell stack voltage was plotted against the current values to produce the I-V curve shown in Fig. 15.

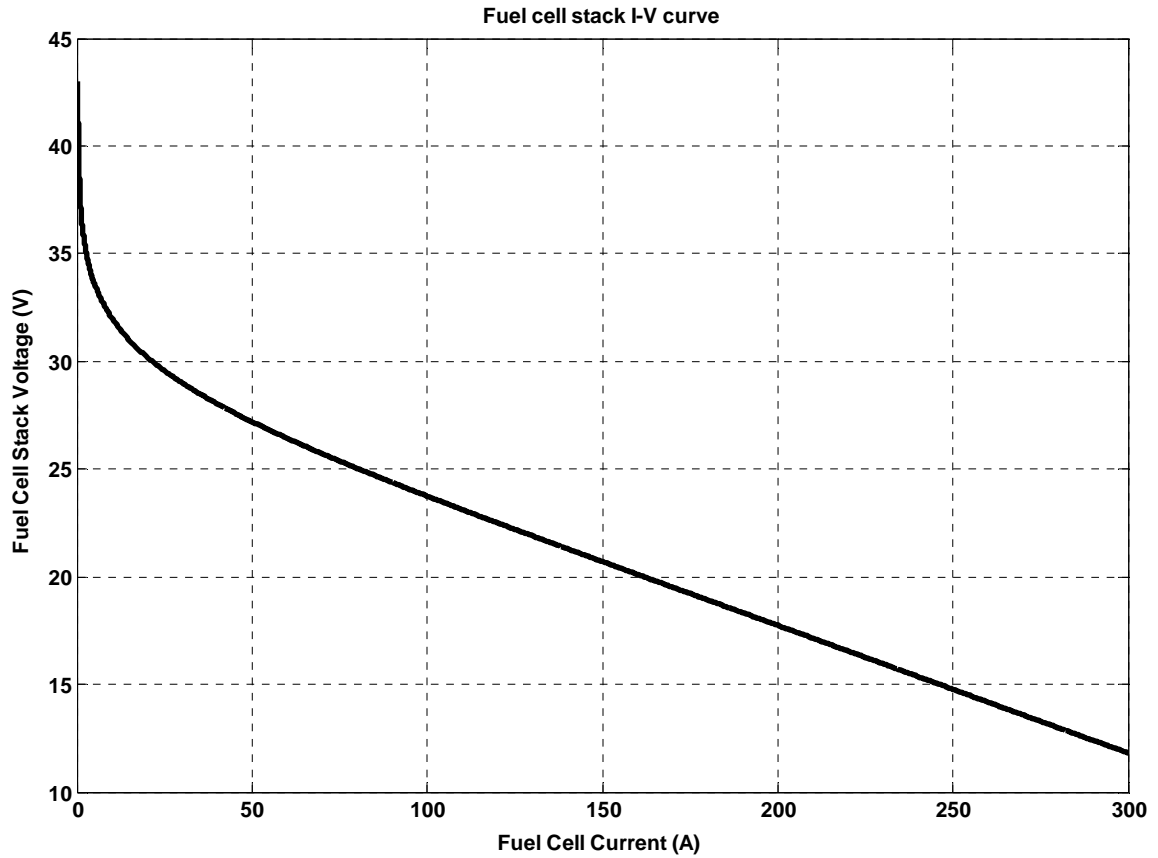


Fig. 15. Fuel cell stack I-V curve from simulation

Note that the I-V curve shows the activation and ohmic polarization regions, as described in Section IV. The concentration region is not shown because the fuel cell does not operate in that region. The stack voltage ranges from 12 to 43 V and will be useful when implementing the dc-dc boost converter controller and selecting ultracapacitors. Similar to the I-V curve, the I-P curve was generated by directly applying the same range of current values and plotting the output power, shown in Fig. 16.

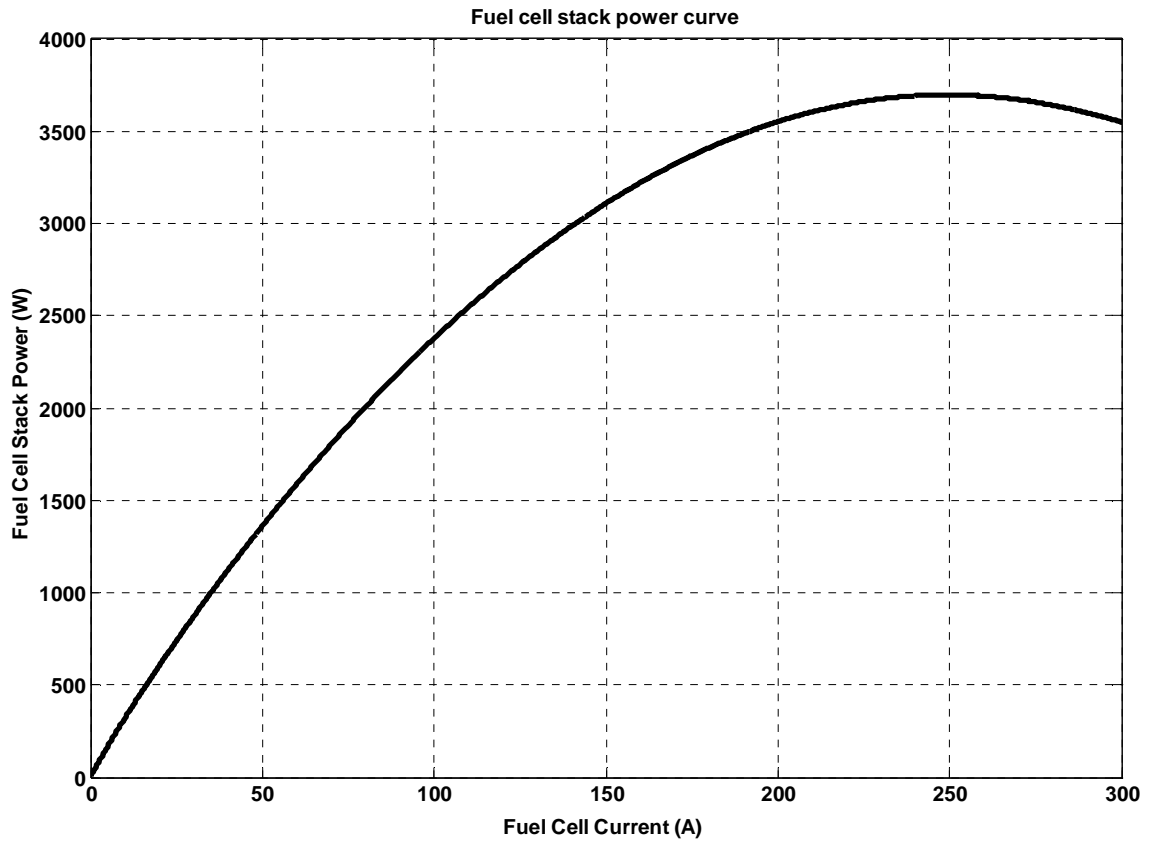


Fig. 16. Fuel cell stack I-P curve from simulation

The fuel cell’s maximum power point occurs at 249 A, producing 3.696 kW. It is not advantageous to operate the fuel cell at currents greater than 249 A, thus setting the upper limit of the current limiter inside the fuel cell stack subsystem.

The fuel cell’s dynamic response may be examined by using the original system model presented in Fig. 11 and applying the following load profile:

Simulation Time (s)	Load Power (W)	Load Resistance (Ω)
0 – 2	1	57,600.0
2 – 7	500	115.0
7 – 12	2000	28.8
12 – 15	1000	57.6

Table 1. Time varying load profile for first case study

Note that in Table 1, the load resistance is inversely related to the load power by the square of the ac RMS voltage. The power demand sent to the fuel cell stack must account for power converter inefficiencies (each at 95%), as shown in Fig. 17, resulting in higher overall power demanded from the fuel cell.

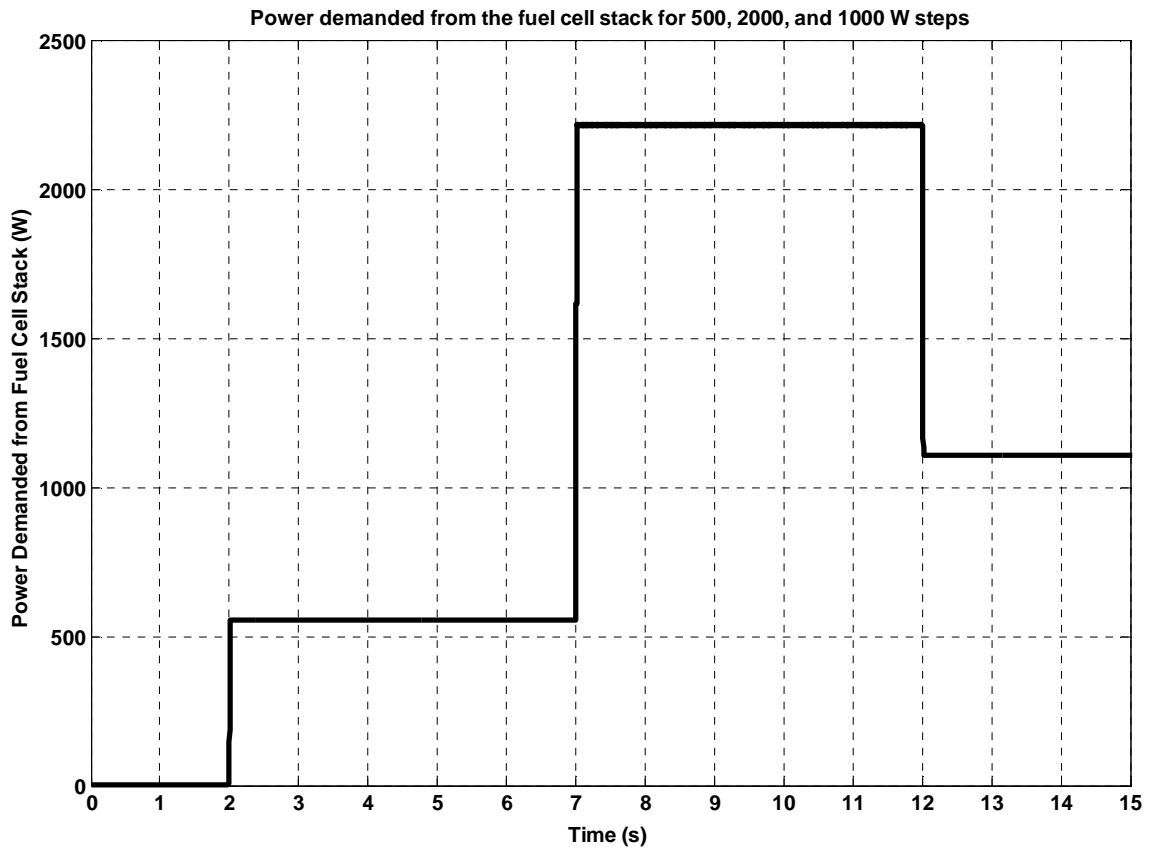


Fig. 17. Power demanded from fuel cell stack for 500, 2000, and 1000 W load steps

Due to the double layer capacitance effect and reactant flow dynamics, the fuel cell stack's voltage and current do not change instantly with a change in power. This phenomenon as it applies to the present load profile is illustrated in Fig. 18.

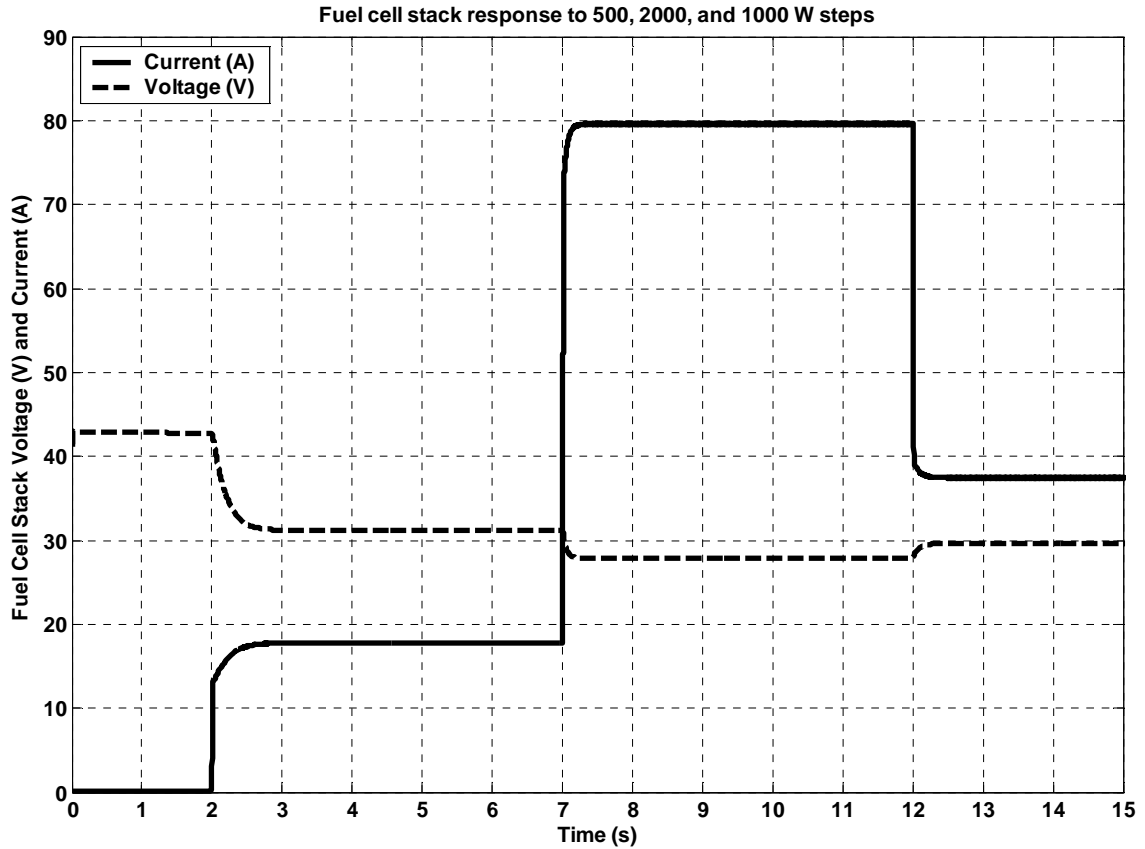


Fig. 18. Fuel cell voltage/current response to 500, 2000, and 1000 W load steps

Even though the voltage and current respond slowly to dynamic loads, their product results in a rapid power response. As long as the load power does not exceed the fuel cell stack's maximum power, the fuel cell presented in this case study will be able to respond adequately to dynamic loads based on the assumed characteristics in Table 1 and Fig. 17 [15].

The first case study may be applied to residential loads that are purely resistive and do not have any transients. Electric stoves, ovens, water heaters, and incandescent light bulbs are likely to fit the step load profile presented in the first case study. However, it is necessary to examine the fuel cell stack's response to transient loads and

loads that exceed the fuel cell stack's maximum power. Such scenarios are presented in the second case study.

A heat pump is an ideal candidate for evaluating the integration of a fuel cell system into a residence, thus serving as the basis for the second case study. Because a heat pump is usually the single largest electric load in a house, it may be used to evaluate a fuel cell system's limitations. When a heat pump starts, it produces a rapid and powerful transient, resulting from the compressor's induction motor starting. The power levels incurred at the peak of the startup transient may exceed 15 kW, far beyond the rating of a residential-size fuel cell. As discussed in Section VII, ultracapacitors are best suited to supply additional power in large quantities but in small bursts. By simulating a fuel cell stack during transient and overload conditions, the necessary supplemental power can be determined, leading to an optimal ultracapacitor selection. This second case study involves two major model changes from the first case study. First, two fuel cell stacks are considered instead of one. The stacks operate in parallel with each other, not changing the overall stack voltage but doubling the current output. Two fuel cell stacks having the same parameters from the first case study will produce a maximum of 7.4 kW. Secondly, an additional subsystem is added to calculate the capacitance (C_{sup}) needed to supply adequate supplementary power (P_{sup}) to the system for a given load profile. The supplemental capacitance subsystem is shown in Fig. 19 and described by (20).

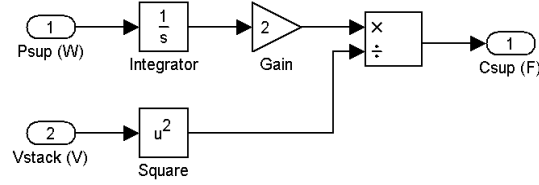


Fig. 19. Supplemental capacitance subsystem

$$C_{\text{sup}} = \frac{2 \cdot \int_{t_{\text{start}}}^{t_{\text{end}}} p_{\text{sup}} dt}{V_{\text{stack}}^2} \quad (20)$$

Equation (20) is based on the energy equation for a capacitor,

$$W = \frac{1}{2} \cdot C \cdot V^2 \quad (21)$$

where W is the energy stored in the capacitor and V is the voltage across the capacitor.

By assuming the capacitor fully discharges, the capacitor's voltage will be driven to zero.

The energy stored in the capacitor can be determined by integrating the supplemental power needed by the system during the transient. The limits of integration, t_{start} and t_{end} , represent the transient start time and end time (when the transient power is met by the fuel cell stack). It is important to address the known limitations of (20) and its affect on the supplemental capacitance result. A capacitor's voltage approaches zero as the capacitor discharges, indicating that a capacitor connected in parallel with a fuel cell stack never fully discharges. Furthermore, each incremental increase in supplemental capacitance alters the fuel cell stack's response and the fuel cell stack's ability to meet the power demand. This characteristic introduces a non-linearity in the model and has been neglected. An iterative approach must be taken to obtain more-accurate capacitance values. Fortunately, the proposed linear model outputs a capacitance higher than needed so that if this model were to be used in practice, the system power demand will be met.

The simulated heat pump that serves as part of the load has the following characteristics:

Line Voltage	240 V ac RMS
Start Current	75 A
Run Current	18 A
Time Constant	0.5 s

Table 2. Heat pump specifications

An equivalent expression for the heat pump power (P_{hp}) may be derived from the characteristics in Table 2,

$$p_{hp} = p_{run} + (p_{start} - p_{run}) \cdot e^{\frac{-t}{\tau_{hp}}} \quad (22)$$

$$p_{hp} = 4.32 + 13.68 \cdot e^{\frac{-t}{0.5}} \quad (23)$$

where p_{run} and p_{start} are the run power and start powers, respectively, determined by the product of the line voltage and corresponding current, assuming unity power factor.

While starting a motor at unity power factor is not realistic, it is necessary to make this assumption to stay consistent with the given load profile. The heat pump startup transient will decay in about five time constants ($5 \cdot \tau_{hp}$), indicating that the heat pump described above will transition from start to run in about 2.5 seconds. In addition to the heat pump, a static load of 1.0 kW is added to the load profile to simulate the base load of a residential dwelling. The load profile is shown in Fig. 20.

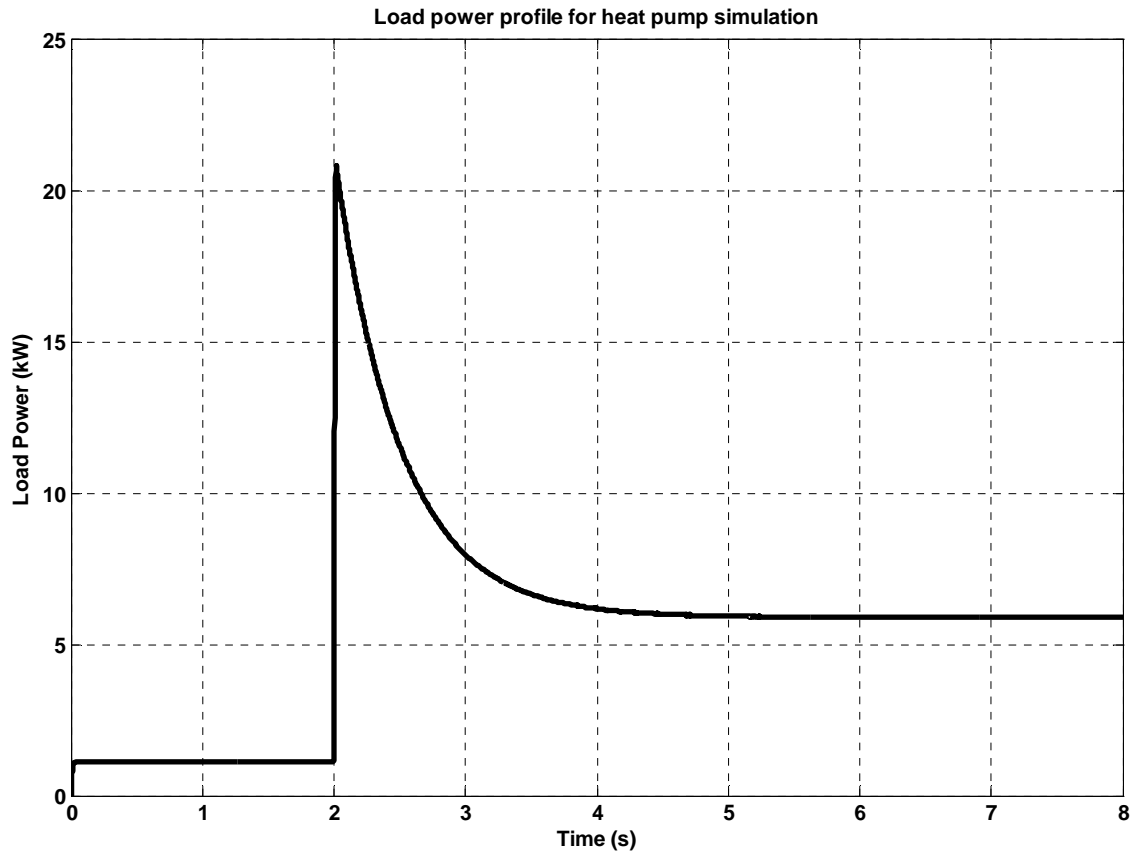


Fig. 20. Load power profile for heat pump simulation

When simulated, the fuel cell stack pair provided the output power shown in Fig. 21.

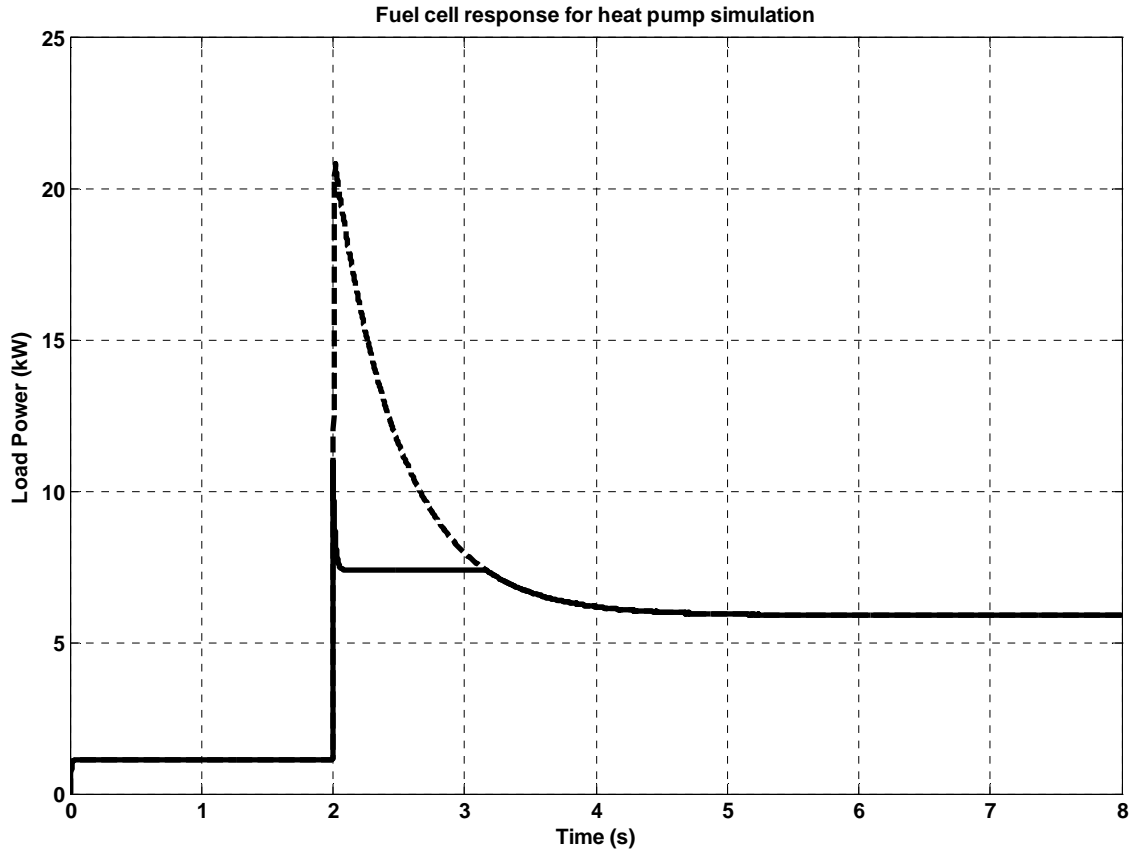


Fig. 21. Fuel cell response to heat pump simulation

The ultracapacitor’s capacitance was determined from the model in Fig. 19 to be 45.9 F to supply all necessary supplemental power to the load. An iterative approach is required to obtain truly accurate results, even though it is not known how much an iterative approach would affect the present value. The analysis presented in both the first and second case studies may be extended to different PEM fuel cell types and simulated with a variety of load profiles.

The fuel cell system model may be adapted for determining battery capacities to aid the fuel cell stack in meeting short-term peak loads. As both startup transients and short-term loads are anticipated to exceed the fuel cell stack’s power limitations,

determining supplemental battery capacities to meet short-term peak loads will follow a similar simulation as the one presented in the second case study. For this reason, the supplemental battery determination simulation was not considered any further.

XI. CONCLUSION

The fuel cell model presented in this text has been examined from many levels. Although many fuel cell types exist, the PEM fuel cell far exceeds other types in development and marketability. The PEM fuel cell stack, along with necessary power conditioning electronics, has been modeled for residential applications. The core of the model centers around the set of equations governing the fuel cell's output voltage and current, accounting for activation and ohmic overpotentials, the double-layer capacitance effect, and reactant flow dynamics. A known load profile may be applied as an input to the model so that the fuel cell stack can be examined for its response. Furthermore, the model can serve as a tool to determine optimal supplemental power sources needed to supply loads with severe startup transients, such as residential appliances that use induction motors. By implementing the model in Simulink, the fuel cell system can be adapted and modified for various other analyses. The material presented in this thesis has created avenues for future work. Future analysis may be performed by applying a load impedance as the system input rather than a load resistance. A load impedance may introduce both real and reactive power demands, leading to varying power factors. A second consideration for future analysis is implementing an iterative procedure to determine supplemental capacitances and to account for nonlinearities. Ultimately, this thesis will allow an engineer to explore fuel cells not only for the advancement of research but also for the betterment of society.

XII. REFERENCES

- [1] EG&G Technical Services Inc., "Fuel Cell Handbook," 7th ed., U.S. Department of Energy, West Virginia, November 2004.
- [2] A. J. Appleby and F. R. Foulkes, *Fuel Cell Handbook*, Van Nostrand Reinhold, New York, 1989.
- [3] Fuel Cell Initiative Advisory Committee, "Fuel Cell Applications and Case Studies," FCIAC Team Report, Texas State Government, Texas, 2002.
- [4] Huann-Keng Chiang, Bor-Ren Lin, and Yuan-An Ou, "Implementation of a Stand-Alone Fuel Cell System for Domestic Applications," National Yunlin University of Science and Technology, Taiwan, 2004.
- [5] M. J. Khan and M. T. Iqbal, "Modelling and Analysis of Electro-chemical, Thermal, and Reactant Flow Dynamics for a PEM Fuel Cell System," *Fuel Cells*, vol. 5, no. 4, pp. 463-475, 2005.
- [6] P. R. Pathapati, X. Xue, and J. Tang, "A New Dynamic Model for Predicting Transient Phenomena in a PEM Fuel Cell System," *Renewable Energy*, vol. 30, no. 1, pp. 1-22, January 2005.
- [7] J. M. Correa, F. A. Farret, L. N. Canha, and M. G. Simoes, "An Electrochemical-Based Fuel-Cell Model Suitable for Electrical Engineering Automation Approach," *IEEE Transactions on Industrial Electronics*, vol. 51, no. 5, pp. 1103-1112, October 2004.
- [8] M. Y. El-Sharkh, A. Rahman, M. S. Alam, P. C. Byrne, A. A. Sakla, and T. Thomas, "A Dynamic Model for a Stand-alone PEM Fuel Cell Power Plant for Residential Applications," *Journal of Power Sources*, vol. 138, no. 1-2, pp. 199-204, November 2004.
- [9] M. J. Khan and M. T. Iqbal, "Dynamic Modelling and Simulation of a Fuel Cell Generator," *Fuel Cells*, vol. 5, no. 1, pp. 97-104, February 2005.
- [10] Gert K. Andersen, Christian Klumpner, Søren Bækthøj Kjær, and Frede Blaabjerg, "A New Power Converter for Fuel Cells with High System Efficiency," *International Journal of Electronics*, vol. 90, no. 11-12, pp. 737-750, November-December 2003.

- [11] M. J. Khan and M. T. Iqbal, "Dynamic Modeling and Simulation of a Small Wind-Fuel Cell Hybrid Energy System," *Renewable Energy*, vol. 30, no. 3, pp. 421-439, March 2005.
- [12] Robert J. Braun, Sanford A. Klein, and Douglas T. Reindl, "Considerations in the Design and Application of Solid Oxide Fuel Cell Energy Systems in Residential Markets," *ASHRAE Transactions*, vol. 110, no. 1, pp. 14-24, 2004.
- [13] J. C. Amphlett, R. F. Mann, B. A. Peppley, P. R. Roberge, and A. Rodrigues, "A Model Predicting Transient Responses of Proton Exchange Membrane Fuel Cells," *Journal of Power Sources*, vol. 61, no. 1-2, pp. 183-188, July-August 1996.
- [14] EG&G Technical Services Inc. and Science Applications International Corp., "Fuel Cell Handbook," 6th ed., U.S. Department of Energy, West Virginia, November 2002.
- [15] M. Y. El-Sharkh, A. Rahman, M. S. Alam, A. A. Sakla, P. C. Byrne, and T. Thomas, "Analysis of Active and Reactive Power Control of a Stand-alone PEM Fuel Cell Power Plant," *IEEE Transactions on Power Systems*, vol. 19, no. 4, pp. 2022-2028, November 2004.

XIII. APPENDIX

Matlab code for simulation parameters and variable initialization:

```
% FUEL CELL PARAMETERS
T = 300;           % K, Temperature
R = 8.314;        % Gas constant
F = 96485;        % Farady's constant
N = 35;           % Number of cells
E0 = 1.229;       % V, Thermodynamical potential
kE = 8.5e-3;      % Temperature correction constant

z1 = -.944;       % Parameters for activation overpotential
z2 = 3.54e-3;
z3 = 7.8e-5;
z4 = -1.96e-4;
z5 = 3.3e-3;      % Parameters for ohmic overpotential
z6 = -7.55e-6;
z7 = 1.1e-6;

A = 232;          % Cell area
Cdl = .035*A;    % Farads

I_max = 249;      % A, determined from I-P curve
I_min = .01;     % A

% REACTANT FLOW PARAMETERS
xH2 = .9999;      % fraction of hydrogen
xO2 = .21;        % fraction of oxygen
xH2O = .01;       % fraction of vapor

Va = .0159;      % Anode volume (m^3)
Vc = .0025;      % Cathode volume
ka = .004;       % Anode flow constant
kc = .001;       % Cathode flow constant

H2_flow = 8;     % slpm
Air_flow = 120;  % slpm
Pambient = 1;    % atm

pH2_max = 5;     % atm
pH2_min = .001;
pO2_max = 5;
pO2_min = .001;
pH2O_max = 5;
pH2O_min = .001;
```

```
% POWER CONVERTER PARAMETERS
Vac_rms = 240;           % V RMS
Vboost_ref = 400;       % V DC
Vac_ref = Vac_rms*sqrt(2); % V magnitude
kP_DC = 5;              % Boost converter proportional constant
kI_DC = 5/2;            % Boost converter integral constant
kP_AC = .05;            % Inverter proportional constant
kI_AC = .05/.015;      % Inverter proportional constant
Eff_Converter = .95 * .95; % percent
```